ESC European Society of Cardiology

Cardiovascular Research (2022) **118**, 2833–2846
https://doi.org/10.1093/cvr/cvab344

Endothelial ARHGEF26 is an angiogenic factor promoting VEGF signalling

Qiuyu Martin Zhu [1,2,3], Bryan T. MacDonald [1], Taiji Mizoguchi[1,3], Mark Chaffin[1], Alison Leed [4], Alessandro Arduini[1], Edyta Malolepsza[5], Kasper Lage[6,7], Virendar K. Kaushik[4], Sekar Kathiresan [1,2,8], and Patrick T. Ellinor [1,3]*

[1]Cardiovascular Disease Initiative, The Broad Institute of MIT and Harvard, 75 Ames Street, Cambridge, MA 02142, USA; [2]Center for Genomic Medicine, Massachusetts General Hospital, Boston, MA, USA; [3]Cardiovascular Research Center, Massachusetts General Hospital, Boston, MA, USA; [4]Center for the Development of Therapeutics, The Broad Institute of Harvard and MIT, Cambridge, MA, USA; [5]Genomics Platform, The Broad Institute of Harvard and MIT, Cambridge, MA, USA; [6]Department of Surgery, Massachusetts General Hospital, Harvard Medical School, Boston, MA, USA; [7]Stanley Center for Psychiatric Research, The Broad Institute of MIT and Harvard, Cambridge, MA, USA; and [8]Verve Therapeutics, Cambridge, MA, USA

Received 13 July 2021; editorial decision 28 October 2021; online publish-ahead-of-print 26 November 2021

Time for primary review: 42 days

See the editorial comment for this article 'ARHGEF26: a new player in vascular endothelial growth factor receptor 2 trafficking', by Anne-Clémence Vion and Gervaise Loirand, https://doi.org/10.1093/cvr/cvac149.

Aims Genetic studies have implicated the *ARHGEF26* locus in the risk of coronary artery disease (CAD). However, the causal pathways by which DNA variants at the *ARHGEF26* locus confer risk for CAD are incompletely understood. We sought to elucidate the mechanism responsible for the enhanced risk of CAD associated with the *ARHGEF26* locus.

Methods and results In a conditional analysis of the *ARHGEF26* locus, we show that the sentinel CAD-risk signal is significantly associated with various non-lipid vascular phenotypes. In human endothelial cell (EC), ARHGEF26 promotes the angiogenic capacity, and interacts with known angiogenic factors and pathways. Quantitative mass spectrometry showed that one CAD-risk coding variant, rs12493885 (p.Val29Leu), resulted in a gain-of-function ARHGEF26 that enhances proangiogenic signalling and displays enhanced interactions with several proteins partially related to the angiogenic pathway. ARHGEF26 is required for endothelial angiogenesis by promoting macropinocytosis of Vascular Endothelial Growth Factor Receptor 2 (VEGFR2) on cell membrane and is crucial to Vascular Endothelial Growth Factor (VEGF)-dependent murine vessel sprouting *ex vivo*. *In vivo*, global or tissue-specific deletion of ARHGEF26 in EC, but not in vascular smooth muscle cells, significantly reduced atherosclerosis in mice, with enhanced plaque stability.

Conclusions Our results demonstrate that ARHGEF26 is involved in angiogenesis signaling, and that DNA variants within *ARHGEF26* that are associated with CAD risk could affect angiogenic processes by potentiating VEGF-dependent angiogenesis.

Keywords coronary artery disease • angiogenesis • atherosclerosis • endothelial cell

1. Introduction

Coronary artery disease (CAD) is the leading global cause of mortality.[1] Current treatment for CAD is almost exclusively directed at reducing plasma cholesterol level or thrombosis. However, despite these advances, CAD is predicted to remain the leading cause of death for the next 20 years.[2] Developing novel, efficacious therapeutic strategies for CAD remains a major public health need.

Understanding the genetic architecture of CAD is essential for discovering new therapeutics. To date, genome-wide association studies (GWASs) have brought the total number of known CAD-associated genetic loci to >160.[3] Of note, only 20% of the loci are located near genes with known roles in regulating lipid risk factors: low-density lipoprotein (LDL), triglyceride-rich lipoproteins or lipoprotein(a).[4] Thus, the vast majority of CAD risk loci are related to largely uncharted 'non-lipid'

* Corresponding author. Tel: +1 617 724 8729, E-mail: ellinor@mgh.harvard.edu

pathways. Understanding these non-lipid pathways may unlock new potential therapeutics for CAD.

One critical non-lipid causal process that participates in all stages of atherosclerosis is angiogenesis. A recent GWAS found that genes involved in angiogenesis were among the most significantly enriched gene sets associated with CAD.[5] Plaque neovascularization is regarded as both the cause and consequence of atherosclerosis in human.[6] Specifically, intramural hypoxia initiates neovascularization, and neovessels in turn promote infiltration of inflammatory cells to the vessel wall leading to non-resolving inflammation. Pathological angiogenesis in human atherosclerotic lesion has been shown to promote plaque progression, instability, and thromboembolic events. Pharmacological agents that inhibit intra-plaque angiogenesis showed promise in animal models to stabilize or even regress plaques independent of lipid-lowering, pointing to angiogenesis as a novel therapeutic target for CAD.[7,8] However, existing therapeutics directly targeting intra-plaque angiogenesis in humans are limited and inconclusive.[9] A major knowledge gap exists in our understanding of the critical genetic elements underlying the angiogenic pathway.[6,10]

We and others have recently found that DNA variants at a non-lipid *ARHGEF26* locus were significantly associated with CAD.[5,11,12] ARHGEF26 (Rho guanine nucleotide exchange factor 26) is a guanine nucleotide exchange factor (GEF) that activates RhoG GTPase by exchanging guanosine diphosphate (GDP) for guanosine triphosphate (GTP).[13,14] Previously, we and others have shown that ARHGEF26 helps form cup-like docking structures in endothelial cell (EC) to aid transendothelial migration of leukocytes,[11,15–17] a critical initial step to the formation of atherosclerosis.[15] However, the role of ARHGEF26 in the vasculature remains to be fully characterized, and the exact causal mechanism by which DNA variants at *ARHGEF26* locus affect risk for CAD remains unknown.

Here, we show that endothelial ARHGEF26 is a critical regulator of angiogenesis and provide mechanistic evidence that a gain-of-function (GOF) variant in *ARHGEF26* may contribute to CAD via angiogenic pathways.

2. Methods

Major resources and extended methods are in the Supplementary material online.

2.1 CRISPR/Cas9 genome editing in TeloHAEC

The pSpCas9(BB)-2A-Neo vector that expresses *SpCas9* and a neomycin resistance (*neoR*) gene was a kind gift from Dr. Guillaume Lettre (Montreal Heart Institute, Canada). An efficient guide sequence 5′-CCGTAATTAGTAACCCGTTG GGG (protospacer adjacent motif; PAM) -3′ targeting Exon 2 of *ARHGEF26* with no predicted exonal off-target cleavage was selected using the Zhang Lab CRISPR Design website (http://crispr.mit.edu/, last accessed 11/21/2021), cloned into pSpCas9(BB)-2A-Neo vector, and confirmed by Sanger sequencing. TeloHAEC was transfected with the vector by nucleofection and cultured for 48 h. Cells were incubated with 200 μg/ml G418 (Thermo Fisher Scientific) to select for neoR for 7 days, after which surviving cells were seeded on 96-well plate at a density of 0.5 cell/well to isolate monoclonal population. Colonies were monitored for 7–14 days, followed by transfer and expansion of individual clones on 24-well plates. Genomic DNA was extracted from individual clones, and the indels at expected cleavage site were examined by sequencing PCR products flanking Exon 2. Mutations were decomposed using the TIDE tool[18] to yield clones with putative biallelic indels. The exact mutation of individual alleles was sequenced by allelic cloning (New England Biolabs). A clone with a homozygous 11-bp frameshift deletion within Exon 2 was expanded as *ARHGEF26-KO* clone, whereas a clone that survived G418-selection but showed no indels at expected DNA cleavage site was expanded as *ARHGEF26-WT* clone. The presence or absence of ARHGEF26 protein in these clones was confirmed by western blot.

2.2 Protein stability assay by cycloheximide chase

To examine intracellular ARHGEF26 protein stability, we performed a semi-quantitative chasing in cells treated with cycloheximide, a *de novo* protein synthesis inhibitor. HEK293 cells were transfected with 3×FLAG-ARHGEF26-WT or 3×FLAG-ARHGEF26-29Leu, cultured for 48 h, and re-plated on one 24-well plate at 1.5×10^5 cells and 500 μl DMEM-GlutaMAX mdium containing 10% fetal bovine serum (FBS) per well. The next day, additional 500 μl medium containing 100 μg/ml cycloheximide (Enzo Life Sciences) was carefully added to produce 50 μg/ml final concentration of cycloheximide in each well. Four wells (2 for 3×FLAG-ARHGEF26-WT and 2 for 3×FLAG-ARHGEF26-29Leu) of cells were harvested each time at 0, 5, 10, 15, 20, and 25 h after cycloheximide treatment. Protein concentration oflysate was normalized by a bicinchoninic acid assay, and 20 μg lysate from each time point was resolved on the same gel by SDS-PAGE. All lanes from SDS-PAGE were first stained with Ponceau S to confirm equal protein input, and then probed for FLAG by western blot.

2.3 2D tube formation assay

The tube formation assay of EC in 2D was performed on a 96-well μ-plate (ibidi, 89646). First, gelation was prepared by loading pre-chilled plate on ice with 10 μl/well Geltrex reduced growth factor matrix (Thermo Fisher Scientific). The plate was placed on a humidified tray at 37°C to solidify the gel for 30 min. A single-cell suspension of EC was added at 1.5×10^5 cells/well in 70 μl medium, and the space outside of the wells was flooded with distilled water. The plate was incubated overnight at 37°C, stained with Calcein-AM (VWR), and imaged on an Axio Vert.A1 inverted fluorescence microscope (ZEISS) with a 5× objective under green fluorescent protein (GFP) channel. The morphology of capillary tubes was analysed using the 'Angiogenesis Analyzer' tool (Carpentier G.; available online: http://image.bio.methods.free.fr/ImageJ/?Angiogenesis-Analyzer-for-ImageJ, last accessed 11/21/2021). A set of optimized parameters were employed for an image of 1024×1024 pixel^2: minimum object size = 50 pixels, minimum branch size = 25 pixels, artifactual loop size = 350 pixels, isolated element size threshold = 25 pixels, master segment size = 30 pixels, and iteration number = 3.

2.4 3D fibrin gel angiogenesis assay

The assay was described previously[19] with modification. Briefly, Cytodex 3 microcarrier beads (Sigma-Aldrich) were hydrated in phosphate buffered saline (PBS). For each experimental group, 2500 beads were incubated with 1×10^6 transfected ECs or TeloHAEC in 4 ml medium in a capped 5-ml round-bottom tube at 37°C. Tubes were gently inverted every 30 min for 4–6 h to coat ECs evenly on bead surface. The bead-cell mixture was incubated on 10-cm petri dishes overnight to allow floating cells to attach, and the coated beads were collected and resuspended in 2.5 ml PBS containing 4.0 mg/ml fibrinogen (Sigma-Aldrich, F8630) and

0.15 U/ml aprotinin (Sigma-Aldrich, A1153). The 2.5 ml bead suspension was gently aliquoted to 8 wells at 250 µl/well. Fresh thrombin stock was diluted to 1.25 U/ml in VascuLife vascular endothelial growth factor (VEGF) medium, and quickly added to each wall at 250 µl/well with a repeating pipette for a final concentration of 0.625 U/ml. The plate was gently shaken to mix, left for 15 min in the hood, and placed in 37°C for 1 h for gelation. Fibroblasts were seeded at 2×10^5 cells/well in VascuLife VEGF medium on top of gel. Sprouting was imaged on an Axio Vert.A1 inverted microscope under bright field. Microvessel morphology of 15 beads per group was analysed using ImageJ as described.[20]

2.5 Biotinylation-based VEGFR2 internalization assay

The semi-quantitative assay was performed as described with modification.[21,22] Briefly, human umbilical vein endothelial cell (HUVEC) was plated on 10-cm dishes and starved in serum-free VascuLife basal medium (Lifeline Cell Technology) for 2 h. HUVEC was labelled with 0.25 mg/ml EZ-Link Sulfo-NHS-SS-Biotin (Thermo Fisher Scientific) in PBS at 4°C for 30 min, and washed with cold PBS containing 50 mM glycine to quench unbound biotin, and twice with cold PBS without glycine. Surface-biotinylated HUVEC was stimulated with VascuLife basal medium containing VEGF (Cell Signaling Technology; 50 ng/ml) and 1% bovine serum albumin (BSA) for 0, 5, 15, or 30 min at 37°C, transferred to 4°C, rinsed three times with cold PBS, and harvested in Pierce IP Lysis Buffer (Thermo Fisher Scientific) containing fresh protease inhibitor. Cell lysate was spun down to remove insoluble debris, normalized to equal input, and processed for IP using streptavidin beads. A rabbit mAb (Cell Signaling Technologies No. 2479) was used in western blot to detect VEGFR2 in total lysate and in the streptavidin pull-down.

2.6 Imaging of internalization of surface VEGFR2

The assay was performed as published[21] with modification. HUVEC was plated on collagen-coated 35-mm glass dishes (MatTek) until near confluent. Cells were starved for 2 h in serum-free VascuLife basal medium, and placed in blocking buffer (VascuLife basal medium containing 1% BSA with 20 mmol/l HEPES) at room temperature for 30 min. Cells were incubated with 1 µg/ml mouse anti-VEGFR2 antibody that recognizes the extracellular domain of VEGFR2 (Abcam, ab9530) for 1 h, briefly rinsed three times with blocking buffer, and immediately soaked in 2 ml pre-warmed VascuLife basal medium containing 1.5 mg/ml lysine-fixable 70-kDa dextran conjugated to Texas Red (Thermo Fisher Scientific, D1864) and VEGF (50 ng/ml). Cells were incubated for 15 min at 37°C without disturbance, briefly washed with ice-cold acidic VascuLife basal medium (pH 2.0) for five times, and immediately fixed in 1% paraformaldehyde (PFA) in PBS. Cells were permeabilized with 0.15% Triton X-100 in PBS for 15 min, blocked with 1% goat serum, and incubated with 1:2000 goat anti-mouse secondary antibody conjugated with Alexa Fluor 488 (Invitrogen) for 1 h at room temperature, stained with 1:10 000 diamidino-2-phenylindole (DAPI; Thermo Fisher Scientific), and washed three times in PBS. Cells were imaged on a confocal microscope (Leica TCS SP8 X) under an HC PL APO CS2 63×/1.40 oil objective, with numerical aperture set at 1.4. Each field was scanned in frame-sequential acquisition mode, in which each channel was captured sequentially with zero crosstalk among fluorophores.

2.7 Experimental animals

Animal experiments were carried out in the Comparative Medicine Facility at the Broad Institute, with approval by the Institutional Animal Care and Use Committees under Protocol ID 0060-07-15-1. All animal procedures conform to the guidelines from Directive 2010/63/EU of the European Parliament on the protection of animals used for scientific purposes and the current NIH guidelines. Euthanasia was performed by CO_2 inhalation as per NIH guidelines. We purchased wild-type (*WT*) C57BL/6J mice (Stock No: 000664) from the Jackson Laboratory. The *Arhgef26−/−* and *Arhgef26-floxed* mice were generated by CRISPR/Cas9 genome editing on C57BL/6J background at the Harvard University Genome Modification Facility. These mice have been successfully bred in our laboratory, and the targeted alleles were transmitted to the progeny following Mendelian ratios. No off-target gene-editing was found by targeted Sanger sequencing of predicted off-target Cas9-cleavage loci (http://crispr.mit.edu/, last accessed 11/21/2021).

2.8 Gene targeting of murine *Arhgef26*

Excision of Exons 4–5 (GEF domain) of murine *Arhgef26* resulted in no functional ARHGEF26 protein.[15] However, a recent report showed that murine Exon 4 harbours a long non-coding RNA that was dysregulated in Rett syndrome[23] with potential cardiovascular complications.[24] Considering Exon 5 alone is essential to the DH domain required for GEF activity, we chose to insert two *loxp* sites flanking only Exon 5 at two evolutionarily unconserved regions (5613-bp apart). Multiple guides were designed (http://crispr.mit.edu/, last accessed 11/21/2021) and tested using the EGxxFP split reporter assay[25] in HEK293 cells, resulting in two guides with the highest efficiency: 5′-GGTTAGCCTGACGAAGAGAC AGG (PAM) -3′ at Introns 4 and 5, and 5′-AGCTACTATGCCGGGCGTGG TGG (PAM) -3′ at Introns 5 and 6. Two crispr RNAs (crRNAs) were produced by Integrated DNA Technologies (IDT). The homology-directed repair (HDR) templates for *loxp* knock-in were two single-stranded DNA donors carrying the *loxp* sequence, mutated PAM, and asymmetrical homology arms[26] to increase knock-in efficiency (PAGE Ultramers, IDT). The CRISPR/Cas9 components were delivered by pronuclear injection of preformed ribonucleoprotein consisting of 30 ng/µl Cas9 protein (PNA Bio), 0.61 pmol/µl crRNA, and 0.61 pmol/µl tracrRNA (IDT) with 10 ng/µl HDR template into one-cell-stage C57BL/6J zygotes.[27] A total of 36 live pups were born, including 6 (16.7%) carrying the 5′-*loxp* and 13 (36.1%) carrying the 3′-*loxp* insertions identified by sequencing of PCR fragments surrounding cleavage sites using tail DNA. To identify the *cis-loxp* alleles, we PCR-amplified 6-kb genomic region spanning the two *loxp* sites for pups carrying both 5′- and 3′-*loxp* insertions. Allelic sequencing of the 6-kb genomic PCR products by PCR cloning (New England Biolabs) identified 1 pup carrying a *cis-loxp* allele, with sequence 100% matching both HDR templates, thereby produced the *Arhgef26-floxed* allele. In addition, 5 (13.9%) pups were found to carry deletion alleles (absence of Exon 5 by cleavage without HDR), thereby produced the *Arhgef26−/−* alleles.

The *Arhgef26* floxed line on C57BL/6J background has been deposited to the Jackson Laboratory as C57BL/6J-*Arhgef26*^{em1Pte}/J (JAX Stock No. 036326).

2.9 Adeno-associated virus (AAV)-induced murine atherosclerosis model

The model was established as described[28] with modification. An *a priori* power calculation was carried out by consulting literature[15,28] and a pilot study to estimate group size of experimental animals. Given that age and

estrogen markedly influence angiogenesis in mice,[29] all experimental mice were age-matched male littermates. Animal randomization was performed by randomly assigning animal ID numbers to AAV-treated group and by blinding the genotypes to the investigators creating and maintaining this model. Proprotein convertase subtilisin/kexin type 9 (*Pcsk9*)-AAV8 carrying mutation D377Y was purchased from Vector Biolabs. Mice were fed on chow diet (PicoLab 5053) prior to AAV injection. At 10 weeks old, mice were given a single intravenous injection of 2.0×10^{11} genome copy of AAV thorough the retro-orbital sinus under inhaled isoflurane anaesthesia (3–4% for induction and 1–3% for maintenance). Visual confirmation of successful injection was immediately conducted by two investigators. Any visible signs of leakage from retro-orbital sinus identified by at least one investigator were considered injection failure, and those animals were excluded by CO_2 inhalation euthanasia. The investigator performing AAV injection was blinded to genotypes. Western diet (Research Diets, D12079Bi) was started the next day for 16 weeks. Blood was collected by retro-orbital bleeding under inhaled isoflurane anaesthesia (3–4% for induction and 1–3% for maintenance) into ethylenediaminetetraacetic acid tubes. Plasma was prepared by centrifugation at 1500 *g* for 15 min for cholesterol level measurement using a fluorometric assay kit (Cayman, 10007640). Mice were transcardially perfused with PBS under inhaled 3% isoflurane anaesthesia at 16 weeks after injection. To measure LDL receptor (LDLR) level, the fresh liver tissue was harvested and homogenized in M-PER buffer supplemented with protease inhibitor using a BeadBug microtube homogenizer (Sigma-Aldrich). Mice were further perfused with 4% PFA. The heart and the entire aorta were dissected and fixed overnight in 4% PFA. The apical 70% of heart was cut offalong the plane perpendicular to the aortic root and discarded. The remaining heart base containing the aortic sinuses were separated from the aorta and embedded in optimal cutting temperature (OCT) compounds (Sakura Finetek, 4583) for sectioning. All harvested animals were subjected to the analyses below without exclusion. A small number (less than five animals per genotype) of stained slides were later excluded due to technical reasons such as section breakage or unsatisfactory staining. The exact numbers of measured animals are reported in legends of Figures 6 and 7.

2.10 Oil red O staining of aorta

Fixed aorta was separate from the heart, rinsed in 60% isopropanol, and placed in fresh oil red O (ORO) working solution (0.3% ORO in 60% isopropanol) for 15 min with gentle agitation. The aorta was washed with 60% isopropanol for 10 min twice and once with PBS. Under a dissection microscope, the adventitial and surrounding fat tissue was thoroughly removed. The branches were cut off, leaving 2 mm each of brachiocephalic artery, left common carotid, left subclavian artery, and common iliac bifurcations. The aorta was cut open along the entire inner curvature and the upper portion of the outer curvature, mounted on glass slides using Aquatex (Sigma-Aldrich, 1085620057), and scanned *en face* using a photo scanner at 3000 dpi resolution. The percentage of ORO area was quantified by Image-Pro Plus (Media Cybernetics).

2.11 Histology

For aortic root lesion analysis, frozen transverse sections of 10-μm thickness were sliced on a cryostat (Leica CM1950) from the bottom up across the entire span of aortic sinuses until reaching the ascending aorta. Every eight equally spaced (70-μm apart) sections were grouped, and stained for ORO (MilliporeSigma, O0625), macrophages/monocytes (Biotin-MOMA2; OriGene SM065B, followed by HRP-Streptavidin SA-5004-1 and DAB reaction SK-4100, Vector Laboratories), Masson's Trichrome (Polysciences, 25088), and vascular smooth muscle cells (VSMC) [α-smooth muscle actin (α-SMA) Cy3; Sigma-Aldrich, C6198], respectively, following the manufacturers' procedures. The slides were counterstained by haematoxylin (VWR, 95057-858) or DAPI, and imaged on a Cell Observer microscope. Quantitative analyses of images were performed by Image-Pro Plus in a blinded manner. All measurements were averaged across the eight equally spaced sections for each mouse.

2.12 Murine aortic ring assay

Mice of 10–12 weeks were transcardially perfused with PBS under deep anaesthesia by inhaled 3% isoflurane. The thoracic aorta was dissected using sterile scissors, trimmed off extraneous fat tissues, and transversely cut into 0.5-mm rings. The aortic rings were extensively washed in PBS and serum-starved at 37°C overnight with 5% CO_2 in Opti-MEM (Thermo Fisher Scientific). Collagen Type I (MilliporeSigma 08-115) was freshly diluted in ice-cold Opti-MEM to 1 mg/ml and transferred to a 96-well plate at 50 μl/well. The rings were carefully submerged in liquid collagen with the luminal axis perpendicular to the bottom of the well. The plate was left undisturbed for 15 min at room temperature and incubated at 37°C for 1 h. The rings embedded in collagen were carefully fed with 150 μl Opti-MEM containing 2.5% FBS and 30 ng/ml VEGF or PBS (vehicle). On Day 4 after embedding, microvessels were stained with CellTracker Green (Invitrogen, C2925) following manufacturer protocol and imaged on an Axio Vert.A1-inverted fluorescence microscope. The relative sprout length (average vessel length/ring diameter) was calculated by ImageJ from 18 rings per treatment (6 rings/mouse × 3 mice/genotype).

2.13 Statistical analyses

Unless specified otherwise, statistical analyses were performed in Prism (GraphPad). Normal distribution of values was assessed by the D'Agostino-Pearson normality test. Statistical difference was calculated by a two-tailed, unpaired Student's *t*-test for two-group comparison, or analysis of variance (ANOVA) followed by Dunnett *post-hoc* tests (one-way ANOVA) or Tukey *post-hoc* tests (two-way ANOVA), for comparisons of three or more groups. *P*-value < 0.05 was considered as statistically significant. All values were expressed as mean ± standard deviation (SD).

3. Results

3.1 Genetic variants at the *ARHGEF26* locus are associated with various non-lipid vascular phenotypes

We initially sought to determine if there were one or more signals associated with CAD at the *ARHGEF26* locus. A GWAS for CAD using an interim release of UK Biobank (4 831 cases and 115 455 controls) identified a leading single nucleotide polymorphism (SNP) rs12493885 (p.Val29Leu) within Exon 2 of *ARHGEF26* at the 3q25.2 locus that was significantly associated with CAD (see Supplementary material online, *Table S1*).[11] rs12493885 is a coding variant that was previously shown to affect endothelial function.[11] A second study replicated the same association signal,[5] and identified an additional SNP rs433903 at the 3q25.2 locus that was significantly associated with CAD[12] (see Supplementary material online, *Table S1*). rs433903 is located 140-kb away from

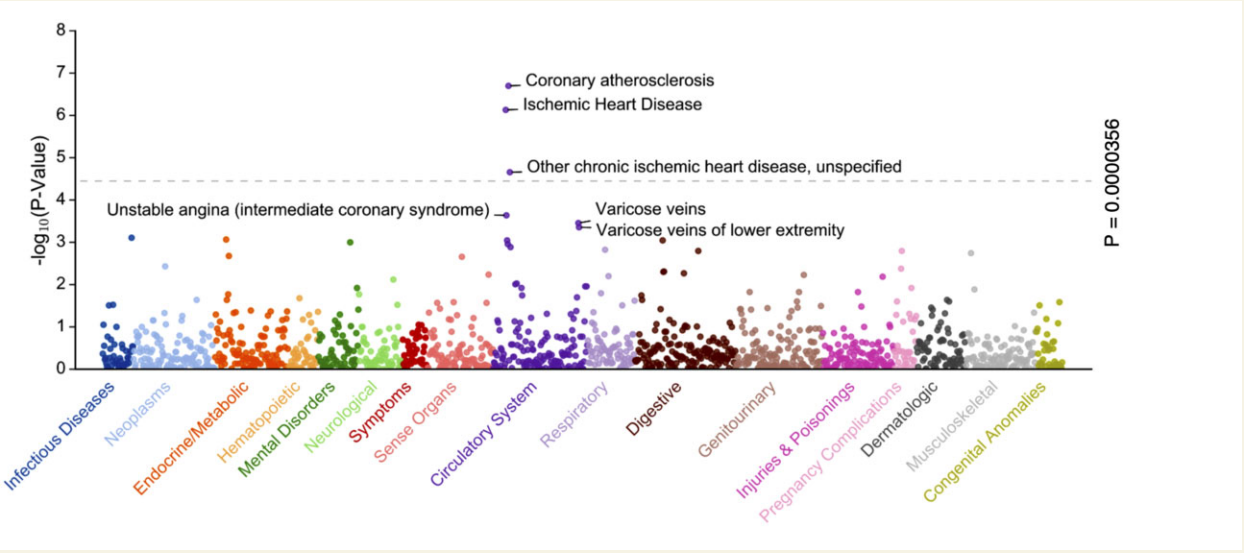

Figure 1 Phenome-wide association results for CAD-risk lead variant rs12493885 at *ARHGEF26* locus. ICD code-based 1403 phenotypes in 17 disease categories in UK Biobank were queried for association with rs12493885 and plotted by -$\log_{10}$ (*P*-value). Phenotypes were declared as significantly associated with rs12493885 if they achieve a Bonferroni-corrected *P*-value < 0.0000356 (0.05/1403 traits) or -$\log_{10}$ (*P*-value) > 4.448 (dashed line). Besides coronary atherosclerosis, rs12493885 is associated with additional phenotypes exclusively within the circulatory system, including significant association with ischaemic heart diseases, and less significant association with unstable angina and varicose veins.

rs12493885 in an intergenic region 3′ to *ARHGEF26*, and is in moderate linkage disequilibrium (LD) with rs12493885 in the 1000 Genomes European population (R^2 = 0.652; the CAD-risk alleles of the two SNPs are linked). To determine whether or not the different sentinel SNPs tag independent CAD-association signals, we performed conditional analyses at the 3q25.2 locus using two different GWAS meta-analyses (see Supplementary material online, *Figure S1*). Despite their imperfect LD, conditioning on either sentinel SNP led to complete dissipation of the CAD-association signal of the other SNP at the 3q25.2 locus, suggesting that the two sentinel SNPs represent one common CAD-association signal.

To explore the mechanistic link between the 3q25.2 locus and CAD, we applied an unbiased phenome-wide association study (PheWAS) approach, searching for potential associations of a given variant with a broad range of phenotypes. This approach is particularly useful for mining causal pathways of diseases with multi-factorial aetiology such as CAD. Using a curated database of 1 403 electronic health record-derived International Classification of Disease (ICD) codes in UK Biobank, we identified several phenotypes, in addition to coronary atherosclerosis, with strong associations with rs12493885, including ischaemic heart disease, unstable angina, and varicose veins (*Figure 1*). These PheWAS-derived phenotypes are distinct from the narrowly defined CAD cases (myocardial infarction and revascularization) in previous GWAS,[11] and therefore may suggest additional functionality of ARHGEF26. Of note, the PheWAS-derived phenotypes emerged solely from the circulatory system (*Figure 1*), and they collectively implicate either a morphogenesis or perfusion defect of the vasculature. We did not identify additional diseases significantly associated with rs12493885, nor did we identify any significant association of rs12493885 with plasma lipids (see Supplementary material online, *Table S2*), further supporting a non-lipid-dependent role of this locus in the vasculature.

We performed an additional PheWAS using the GeneATLAS database containing 778 traits of 452 264 UK Biobank participants. rs12493885 was associated with similar vascular traits that reached phenome-wide significance ($P < 6.427 \times 10^{-5}$; chronic ischaemic heart disease and ischaemic heart disease) or near-phenome-wide significance ($P = 7.6415 \times 10^{-5}$; angina pectoris; Supplementary material online, *Table S3*).

Together, these results suggest CAD-risk genetic variants at the 3q25.2 locus are associated with non-lipid vascular phenotypes. One hypothesis for such association is a role of ARHGEF26 in angiogenesis.

3.2 CAD-risk coding variant Val29Leu differentially interacts with molecules involved in angiogenic processes

We have previously shown that the leading CAD-risk variant rs12493885 (p.Val29Leu) altered ARHGEF26 protein function.[11] Ectopic expression of the mutant ARHGEF26-29Leu (encoded by risk allele C) in vascular endothelial and smooth muscle cells led to a variety of inflammatory phenotypes that constantly exceeded the WT protein, supporting 29Leu as a GOF allele. However, our understanding of the exact GOF mechanism remains limited. Given that no gene-regulatory effect from the risk haplotype was found in human coronary arteries,[11] and that the GDP-GTP exchange activity of ARHGEF26 was unaffected by the 29Leu allele,[11] we examined other aspects of the ARHGEF26 protein that could be impacted by this variant, namely: (i) protein stability, (ii) subcellular localization, and (iii) protein-protein interactions.

First, we tested WT and 29Leu ARHGEF26 protein stability by a degradation chase assay and found the 29Leu mutant ARHGEF26 displayed a longer half-life than WT protein (see Supplementary material online, *Figure S2*). The increase in ARHGEF26 protein stability could partially contribute to a GOF phenotype of the 29Leu allele.

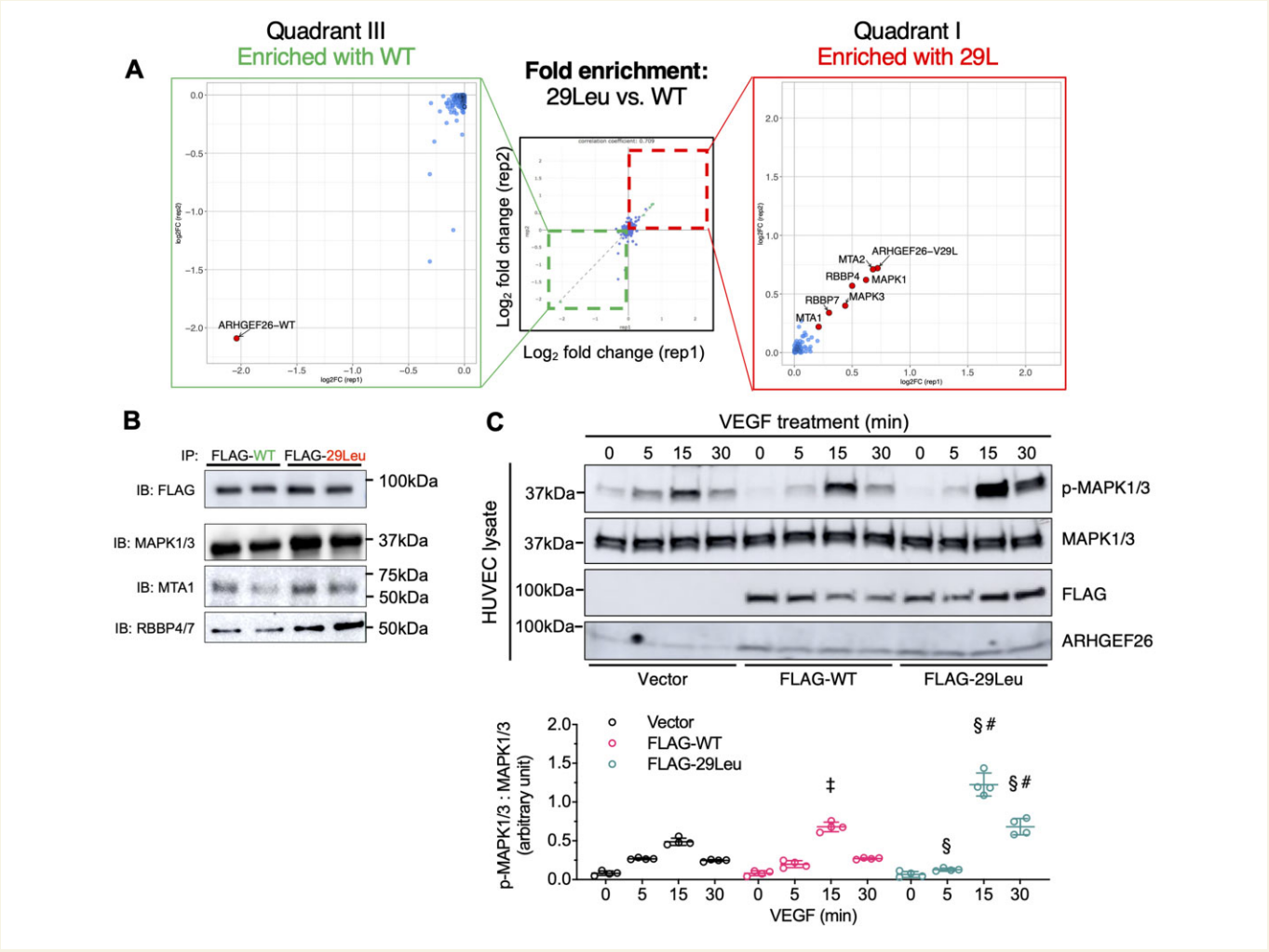

Figure 2 GOF variant Val29Leu of ARHGEF26 differentially interacts with angiogenic factors and enhances pro-angiogenic MAPK signalling. (*A*) Scatterplot showing relative enrichment of proteins with FLAG-ARHGEF26-29Leu (Quadrant I) compared with FLAG-ARHGEF26-WT (Quadrant III) identified by immunoprecipitation and quantitative mass spectrometry from HEK293 cells. Biological replicates from two independent experiments are plotted on the *x*- and *y*-axes, respectively. (*B*) Confirmatory western blot of proteins IP with anti-FLAG antibody from HEK293 cells expressing FLAG-ARHGEF26-29Leu compared with FLAG-ARHGEF26-WT. Stronger band intensity was observed for MAPK1/3, MTA1, and RBBP4/7 by immunoblot (IB). Each blot represents one out of three biological replicates conducted for each IP. (*C*) Overexpressing FLAG-ARHGEF26-29Leu led to significantly higher pro-angiogenic phosphorylation of MAPK1/3 than FLAG-ARHGEF26-WT. HUVEC receiving an empty vector or FLAG-tagged ARHGEF26-WT or ARHGEF26-29Leu was stimulated with VEGF for 0, 5, 15, or 30 min and subjected to immunoblotting analysis using antibodies against MAPK1/3 (phosphorylated or total). Each blot represents one of four independent experiments. Bar graphs below show quantification of the IBs ($n = 4$ blots per column). Multiplicity adjusted $P < 0.05$ (‡, FLAG-WT vs. Vector; §, FLAG-29Leu vs. Vector; #, FLAG-29Leu vs. FLAG-WT) by two-way ANOVA (Tukey); error bars, mean ± SD.

Secondly, since the 29Leu variant is located in a predicted nuclear localization signal (NLS; see Supplementary material online, *Figure S3A*),[13] we examined the subcellular localization of WT and 29Leu ARHGEF26 by imaging. We constructed enhanced green fluorescent protein (EGFP)-ARHGEF26-WT and EGFP-ARHGEF26-29Leu vectors and over-expressed them in HUVECs. Live cell imaging revealed that both EGFP-ARHGEF26-WT and EGFP-ARHGEF26-29Leu were primarily located in the cytoplasm in a diffuse pattern, with prominent EGFP intensity at membrane ruffles[14] (see Supplementary material online, *Figure S3B*). The fluorescent intensity was minimal at the nucleus with no appreciable difference between WT and 29Leu. These results do not support a functional NLS near 29Leu, and suggest that the subcellular localization of ARHGEF26 is not affected by the 29Leu variant.

A third possible consequence of a coding variant may be disrupted protein–protein interaction. To explore this possibility, we overexpressed WT or 29Leu ARHGEF26 with a FLAG-tag in HEK293 cells for <24 h to minimize difference in bait abundance, immunoprecipitated (IP) ARHGEF26 using an anti-FLAG antibody, and compared the protein interactome between WT and 29Leu by highly sensitive, quantitative mass spectrometry. We found that the vast majority of protein interactors were equally enriched in both WT and 29Leu pull-downs, indicating minimal stoichiometric skew that would have otherwise been caused by a more stable 29Leu bait (*Figure 2A*, blue dots surrounding the origin).

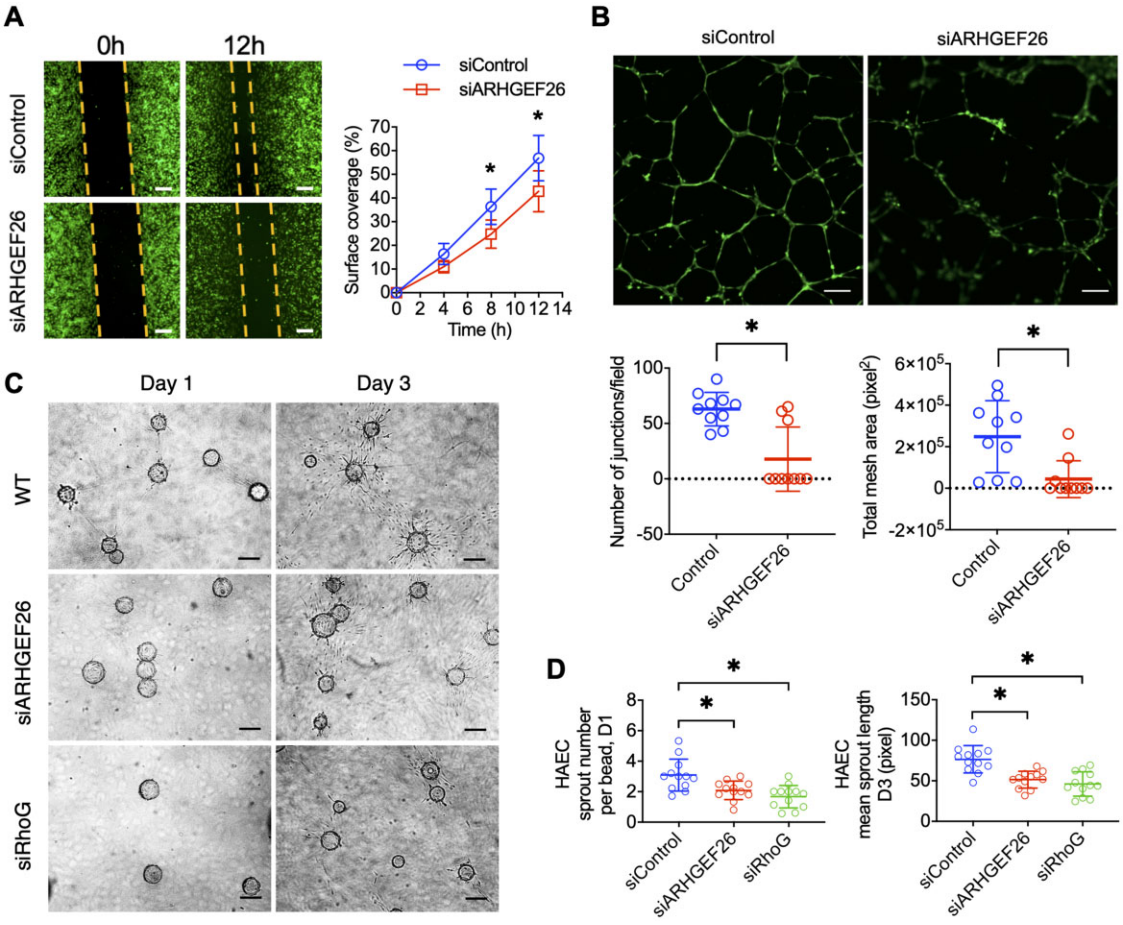

Figure 3 Endothelial ARHGEF26 promotes angiogenesis *in vitro*. (*A*) Significantly reduced wound healing in HAEC receiving siRNA against ARHGEF26 (siARHGEF26) compared with control (siControl). Representative of three independent experiments, with two images captured per experiment per time point ($n = 6$ independent measurements). Scale = 200 μm. *Multiplicity adjusted $P < 0.05$ by Tukey *post-hoc* tests from two-way ANOVA [$F = 3.341$, degree of freedom (DF) = 3]. (*B*) Capillary tube formation in Matrigel was impaired in HAEC receiving siARHGEF26, measured by number of junctions per field and total mesh area. Representative of two independent experiments, with five images captured per experiment per time point ($n = 10$ independent measurements). Scale = 100 μm. *$P < 0.05$ by two-tailed, unpaired Student's *t*-test ($t = 4.374$, DF = 18 for number of junctions per field; $t = 3.309$, DF = 18 for total mesh area). (*C*) 3D tube formation assay in fibrin gel using HAEC-coated beads at Days 1 and 3. Cells were treated with siControl, siARHGEF26, or siRNA against RhoG (siRhoG). Representative of three independent experiments. Scale = 200 μm. (*D*) Quantification of endothelial sprout number per bead (Day 1) and mean sprout length (Day 3) showing that transient knockdown of ARHGEF26 or RhoG by siRNA impaired vasculature formation in the 3D tube formation assay. Five images were captured per experiment per time point from three independent experiments ($n = 12$ independent measurements). *Multiplicity adjusted $P < 0.05$ by Dunnett *post-hoc* tests from one-way ANOVA ($F = 9.425$, DF = 2 for sprout number per bead; $F = 15.36$, DF = 2 for mean sprout length). Error bars, mean ± SD.

However, a subset of protein species showed significantly stronger enrichment with the 29Leu bait than with the WT bait in two biological replicates, including MAPK1/3, Metastasis Associated (MTA) isoforms, and RB Binding Protein (RBBP) isoforms (*Figure 2A*, red dots in Quadrant I). The differential interaction was confirmed by post-IP western blot showing consistently stronger pull-down of the respective preys by the 29Leu bait than by WT (*Figure 2B*). Notably, these differential protein interactors have been commonly implicated in critical angiogenic processes, including VEGF signalling, Notch signalling, HIF-1α response to hypoxia, EC survival and proliferation, and tumour angiogenesis (see Supplementary material online, *Table S4*). Such common association points to a potential connection between *ARHGEF26* and angiogenesis. We further searched for a mechanistical link between the differential protein interactors of 29Leu and known endothelial angiogenic pathways, focussing on the well-characterized VEGF-induced MAPK signalling.[21] EC overexpressing WT and 29Leu ARHGEF26 both showed enhanced pro-angiogenic phosphorylation of MAPK1/3 after 15-min VEGF treatment. Notably, 29Leu led to significantly higher phosphorylation of MAPK1/3 than WT at 15 and 30 min, consistent with an enhanced VEGF signalling that may lead to potentially pro-angiogenic phenotypes (*Figure 2C*).

3.3 Endothelial ARHGEF26 promotes angiogenic capacity *in vitro*

Prompted by the phenotypes associated with ARHGEF26 in PheWAS, we tested the hypothesis that ARHGEF26 regulates endothelial cell

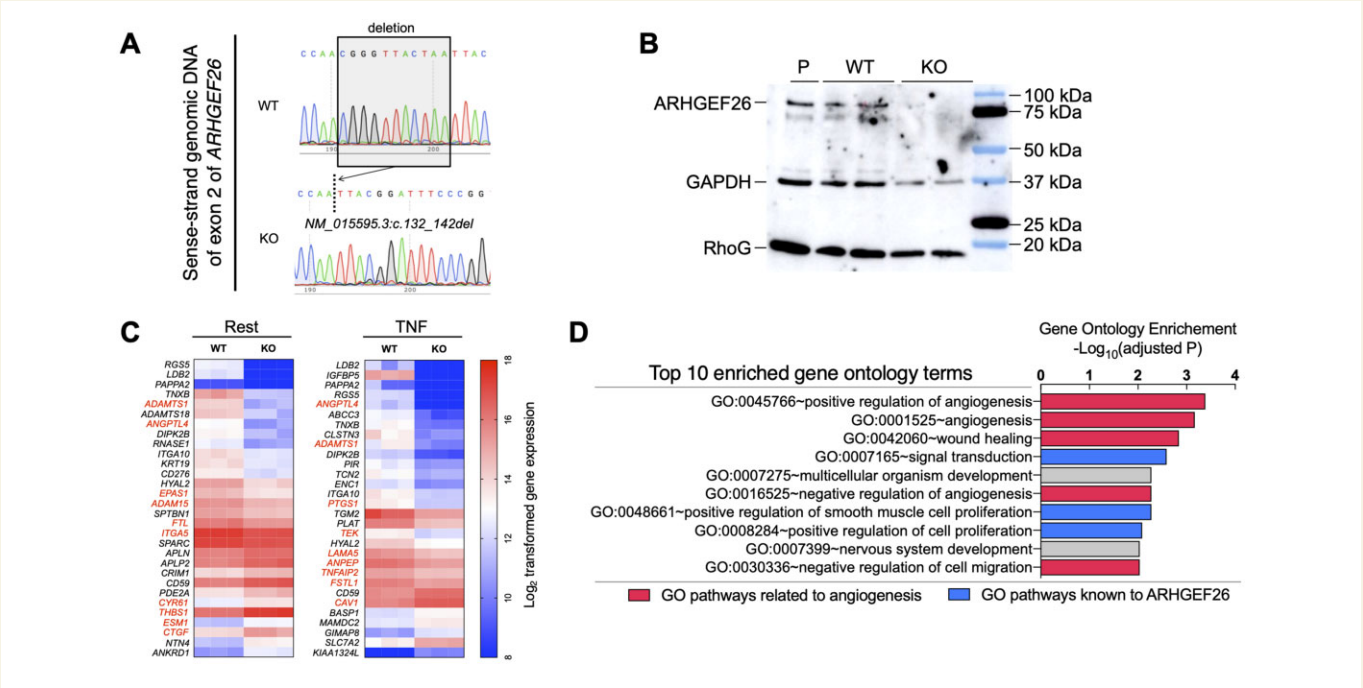

Figure 4 ARHGEF26 interacts with an angiogenic transcriptional program in EC. (*A*) Sanger sequencing of genomic DNA from CRISPR/Cas9-edited TeloHAEC. An 11-nucleotide (nt) fragment was deleted from Exon 2 of *ARHGEF26* in KO cells. (*B*) Multiplex western blot of lysate from parent (P; no gene editing), WT (receiving gene editing and clonal selection with no cleavage) and KO (receiving gene editing and clonal selection with 11-nt homozygous deletion) TeloHAEC using antibodies against ARHGEF26, RhoG, and Glyceraldehyde-3-Phosphate Dehydrogenase (GAPDH, loading control). (*C*) Heatmaps showing the top 30 DEGs (excluding *ARHGEF26*) by RNA-seq of WT vs. KO TeloHAEC at resting and TNF-α-treated conditions, ranked by adjusted *P*-value ($n = 3$ biological replicates per condition per genotype). Genes known to participate in angiogenesis were shown in red symbols. (*D*) Top 10 most significantly enriched GO terms among all DEGs from RNA-seq at TNF-α-treated condition, ranked by -$\log_{10}$ (adjusted *P*). Note: GO terms related to angiogenesis (red) were the most enriched pathways besides those previously known to ARHGEF26 (blue).

angiogenic process *in vitro*. We knocked-down ARHGEF26 in primary human aortic endothelial cells (HAECs) by small interfering RNA (siRNA). ARHGEF26 depletion resulted in significantly impaired endothelial angiogenic capacity, as measured by the wound healing assay (*Figure 3A*) and 2D capillary tube formation assay (*Figure 3B*).

Since angiogenesis is a multi-stage process during which activated ECs sprout, migrate, proliferate, align, form tube, and anastomose, we performed a 3D fibrin gel angiogenesis assay that reproduces these steps in order to systematically capture the morphologic impact by ARHGEF26. We attached primary HAEC on the surface of collagen-coated microcarrier beads and embedded the coated beads in fibrin gel to allow vessel sprouting (*Figure 3C*). Quantitative analyses showed that knockdown of *ARHGEF26* by siRNA inhibited vasculature formation in 3D compared with the control EC, as measured by sprout number per bead on Day 1, and mean sprout length on Day 3. Silencing *RhoG* displayed similar effects as ARHGEF26 siRNA (*Figure 3D*). These results further support an essential role of endothelial ARHGEF26 in vascular tube formation, an effect likely dependent on RhoG.

Taken together, these results suggest ARHGEF26 promotes endothelial cell angiogenic processes *in vitro*.

3.4 Endothelial ARHGEF26 regulates angiogenic genes transcription and pathways

To overcome the transient effect of siRNA, we generated a stable human *ARHGEF26*-knockout (KO) EC line by applying CRISPR/Cas9 gene editing in a telomerase-immortalized, diploid human endothelial cell line TeloHAEC, which created 11-neocleotide homozygous frameshift deletion in Exon 2 of *ARHGEF26* (*Figure 4A*). Comparing with the parent (P; no gene editing) or WT (receiving gene editing but no DNA cleavage) TeloHAEC, homozygous *ARHGEF26*-KO (receiving gene editing and successful cleavage) cells produced no detectable ARHGEF26 protein (*Figure 4B*). Importantly, the expression of RhoG, the direct downstream target of ARHGEF26, remains unchanged in *ARHGEF26*-KO TeloHAEC (*Figure 4B*). The stable *ARHGEF26*-KO cells allowed us to extend the window of the 3D fibrin gel angiogenesis assay up to 5–7 days. Consistent with the siRNA effect in primary EC (*Figure 3C and D*), TeloHAEC showed a significant reduction of sprouting at Days 1 and 3, and total vessel area at Day 5 by stable ARHGEF26 depletion (see Supplementary material online, *Figure S4*), further indicating a critical role of ARHGEF26 in endothelial angiogenic processes.

We next searched for the molecular basis underlying the angiogenic machinery affected by ARHGEF26 in ECs. We first explored the impact of *ARHGEF26* depletion by examining the transcriptional profiles of TeloHAEC cultured at resting condition or under a pro-atherogenic stimulation by tumour necrosis factor alpha (TNF-α). RNA sequencing of TeloHAEC identified thousands of differentially expressed genes (DEGs) between the WT and *ARHGEF26*-KO cells. A focussed analysis of the top 30 significant DEGs at both resting and TNF-treated conditions revealed that these top DEGs consist largely of genes known to participate in angiogenesis (*Figure 4C*). Furthermore, pathway analyses of

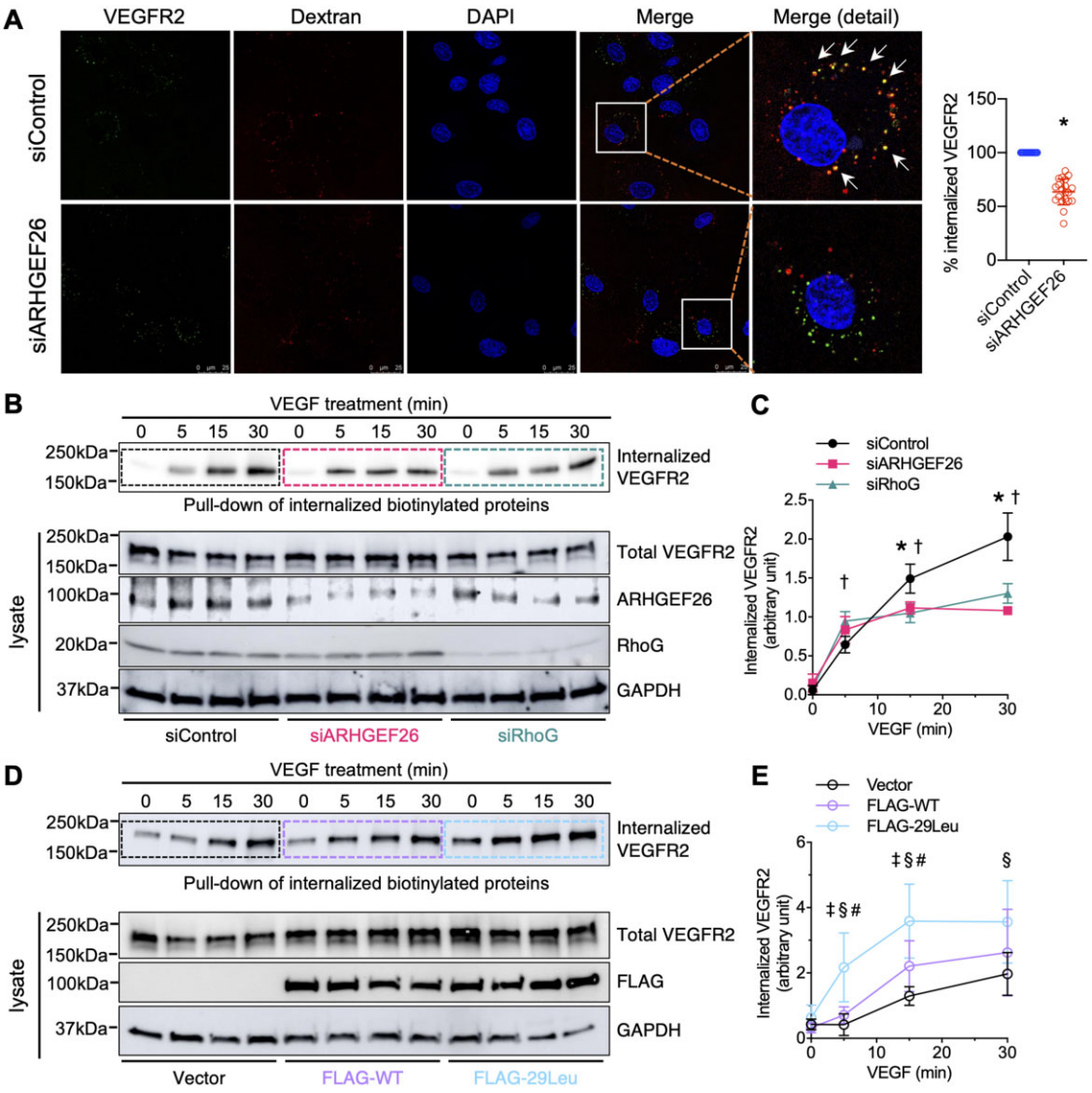

Figure 5 ARHGEF26 promotes VEGF signalling in EC. (*A*) VEGF-dependent macropinocytosis of VEGFR2 requires ARHGEF26. HUVEC receiving siControl or siARHGEF26 was labelled with a mouse anti-VEGFR2 extracellular domain antibody, and incubated at 37°C to allow VEGFR2 internalization in the presence of VEGF and 70-kDa dextran. After washing off unbound antibodies, internalized VEGFR2 was fluorescently labelled with an anti-mouse secondary antibody (green) and inspected using confocal microscopy for co-localization with 70-kDa dextran (red), a marker for macropinosome. Quantification shows significantly reduced yellow macropinocytosomes containing both VEGFR2 and dextran (arrows) by siARHGEF26 treatment ($n = 20$ cells per treatment). Scale = 25 µm. *$P < 0.05$ by two-tailed, unpaired Student's *t*-test ($t = 2.952$, DF = 19). (*B*–*E*) Western blot analysis of VEGFR2 internalization following cell surface biotinylation, VEGF stimulation, and streptavidin-pull-down of internalized surface-biotinylated proteins. HUVEC was treated with siControl, siARHGEF26 or siRhoG (*B* and *C*). Alternatively, HUVEC was transfected with an empty vector or FLAG-tagged ARHGEF26-WT or ARHGEF26-29Leu (*D* and *E*). (*B* and *D*) Blots show internalized surface VEGFR2, as well as proteins in total lysate at the indicated times. Each blot represents one of eight independent experiments. (*C* and *E*) Quantification of VEGFR2 internalization at the indicated times following VEGF stimulation ($n = 8$ independent blots per time point). Multiplicity adjusted $P < 0.05$ (*, siARHGEF26 vs. siControl; †, siRhoG vs. siControl; ‡, FLAG-WT vs. Vector; §, FLAG-29Leu vs. Vector; #, FLAG-29Leu vs. FLAG-WT) by two-way ANOVA [Tukey; $F = 45.66$, DF = 6 for (*C*); $F = 3.174$, DF = 6 for (*E*)]. Error bars, mean ± SD.

all significant DEGs in TNF-treated cells showed that among the top 10 most significantly enriched gene ontology (GO) terms, 5 (50%) are GO terms directly related to angiogenesis, including the top 3 most significantly enriched GO terms among all (*Figure 4D*).

Together, the significant enrichment of angiogenesis-related DEGs and GO terms by stable ARHGEF26 depletion supports its critical role in endothelial angiogenesis.

3.5 ARHGEF26 is crucial to VEGF signalling in EC

Recent reports show that macropinocytosis of cell-surface VEGFR2 upon VEGF binding is absolutely essential to delivering signalling complexes of the receptor to downstream targets including MAPK1/3 and Akt, which are required for endothelial angiogenic responses.[21] Since

ARHGEF26 has been shown to promote macropinocytosis in fibroblasts,[14] we examined the effect of ARHGEF26 on cell-surface VEGFR2 trafficking in EC.

In HUVEC, treatment by VEGF led to internalization of antibody-labelled surface VEGFR2 (*Figure 5A*, green in siControl) in cytoplasmic vesicles that were positive for high-molecular-mass dextran, an established cargo and marker of macropinosomes (*Figure 5A*, red in siControl, merged channel), confirming a previously characterized VEGFR2 internalization route through macropinocytosis.[21] However, silencing of ARHGEF26 caused a marked decrease of surface-labeled VEGFR2 co-localized in dextran-positive vesicles along with a lower number of total dextran-positive vesicles (*Figure 5A*, siARHGEF26 and quantification), indicating impaired VEGFR2 internalization through macropinocytosis by ARHGEF26 knockdown.

We further tested the effect of ARHGEF26 and its downstream target RhoG on the internalization of cell-surface VEGFR2 by a semi-quantitative biotinylation-based receptor internalization assay. Cell-surface VEGFR2 on HUVEC was biotinylated and immediately stimulated with VEGF for varying time to induce VEGFR2 internalization. The internalized, biotinylated surface receptors can be pulled-down using streptavidin beads to allow quantification. Quantification of biotinylated surface VEGFR2 showed that silencing of either ARHGEF26 or RhoG significantly inhibited the internalization of cell-surface VEGFR2 after 15–30 min VEGF treatment (*Figure 5B and C*). Conversely, overexpression of ARHGEF26 significantly increased the internalization of VEGFR2. Notably, overexpression of ARHGEF26-29Leu led to significantly higher internalization of cell-surface VEGFR2 than WT (*Figure 5D and E*). The enhanced VEGFR2 internalization is consistent with our previous observation of increased phosphorylation of MAPK1/3 by 29Leu (*Figure 2C*), which is a downstream signalling step for which macropinocytosis of VEGFR2 is absolutely essential.[21]

Taken together, the microscopy- and biotinylation-based approaches consistently demonstrate that ARHGEF26 is required for the macropinocytosis of VEGFR2, an essential step to VEGF-dependent angiogenesis in EC.

3.6 Deletion of ARHGEF26 in EC, but not VSMC, reduces atherosclerosis in mice

Prior studies showed that global *Arhgef26* deletion in *Apoe*−/− mice reduced atherosclerosis.[15] A more recent study showed ARHGEF26 in VSMC may participate in vascular injury response.[30] Since the tissue-specific role of ARHGEF26 in CAD pathogenesis has never been resolved, we engineered a targeted *Arhgef26* allele in mice by inserting two *loxp* sites flanking Exon 5, a critical exon required for GEF activity, with CRISPR/Cas9 (see Supplementary material online, *Figure S5A*).[27,31] Tissue-specific deletion of *Arhgef26* was achieved in EC and VSMC by crossing floxed mice with *Tek-Cre* and *Tagln-Cre* lines, respectively. For comparison, we also reproduced a global *Arhgef26*-null allele by deleting Exon 5 (see Supplementary material online, *Figure S5A*). Targeting Exon 5 resulted in undetectable ARHGEF26 protein in mice (see Supplementary material online, *Figure S5B*).

We established an efficient murine atherosclerosis model by a single injection of GOF *Pcsk9*-AAV8 (D377Y) followed by 16-week western diet, which resulted in undetectable LDLR in murine liver and markedly increased plasma cholesterol levels (*Figure 6A and B* and see Supplementary material online, *Figure S5C* and *D*). Consistent with prior studies,[15] global *Arhgef26*−/− mice showed significantly reduced aortic atherosclerosis compared with WT in our new model (*Figure 6C–E*). Notably, deletion of *Arhgef26* in EC, but not VSMC, reduces atherosclerosis in mice (*Figure 6C–E*). The magnitude of reduction of atherosclerotic lesion by EC-specific *Arhgef26* deletion was comparable to that by global *Arhgef26* deletion. Importantly, *Arhgef26* depletion *per se* had no effect on plasma cholesterol levels (see Supplementary material online, *Figure S5D*). Together, these results suggest an endothelial-specific role of ARHGEF26 that determines the atherosclerotic burden *in vivo*.

3.7 ARHGEF26 regulates angiogenesis and plaque stability in mice

Finally, to test the role of ARHGEF26 in angiogenesis in a more physiological context, we isolated aortic rings from WT and *Arhgef26*−/− mice and compared their angiogenic capacity by a sprouting assay in the presence of VEGF (*Figure 7A*). When compared with WT, aortic rings from *Arhgef26*−/− mice displayed significantly impaired angiogenesis *ex vivo*, measured by the relative sprout length of microvessels (*Figure 7B*).

Neovascularization is a fundamental contributor to plaque remodelling. Accordingly, we examined the plaque morphology at the aortic root in WT- and EC-specific *Arhgef26*−/− mice, taking into account the content of monocyte/macrophage (*Figures 6C and 7C*), lipid (*Figure 6C*), collagen and VSMC (*Figure 7D*). The vulnerability index, calculated as the ratio of (macrophage content % + lipid content %)/(collagen content % + smooth muscle cell content %), was significantly lower in EC-specific *Arhgef26*−/− mice (*Figure 7E*).

Together, these results indicate ARHGEF26 promotes angiogenesis *ex vivo*, and endothelial ARHGEF26 regulates atherosclerotic plaque composition and stability.

4. Discussion

Human genetics has the potential to illuminate pathogenic mechanisms that can be therapeutically manipulated to lower disease risk. Although the benefit of leveraging genetic information to guide the identification of therapeutic targets is enormous, challenges exist on the path from identifying variants associated with CAD to finding the causative gene(s). Here, we present mechanistic findings that a gene associated with the risk of CAD, *ARHGEF26*, promotes endothelial angiogenesis. Phenotypic associations with a coding variant within *ARHGEF26* point to a lipid-independent role in the vasculature. ARHGEF26 is essential to VEGF-induced angiogenesis in human EC and in mice. ARHGEF26 deficiency in EC, but not VSMC, protects mice from atherosclerosis and influences plaque morphology. Although our data does not establish a causal relationship between enhanced leukocyte trafficking and angiogenesis, the crosstalk between these two pathways can synergistically promote atherosclerosis via increased leukocytes to create a pro-angiogenic milieu, and via enhanced angiogenesis to deliver more leukocytes to further remodel the plaque. Both mechanisms converge on a common therapeutic hypothesis that inhibiting ARHGEF26 in EC may be beneficial for treating CAD.

Our present data are significant because identifying the mechanism through which the CAD-risk variants at 3q25.2 locus affect ARHGEF26 function is an important step toward leveraging genetic variants to mitigate CAD risk. In a conditional analysis we found that the CAD-association is due to one common signal tagged by a coding variant, rs12493885 (p.Val29Leu), within *ARHGEF26*. The directionalities of the phenotypic association and functional effects of this variant align in our observation; namely, the 29Leu allele is associated with higher CAD risk, a GOF protein, and enhanced CAD-causal phenotypes.[11] Aside from

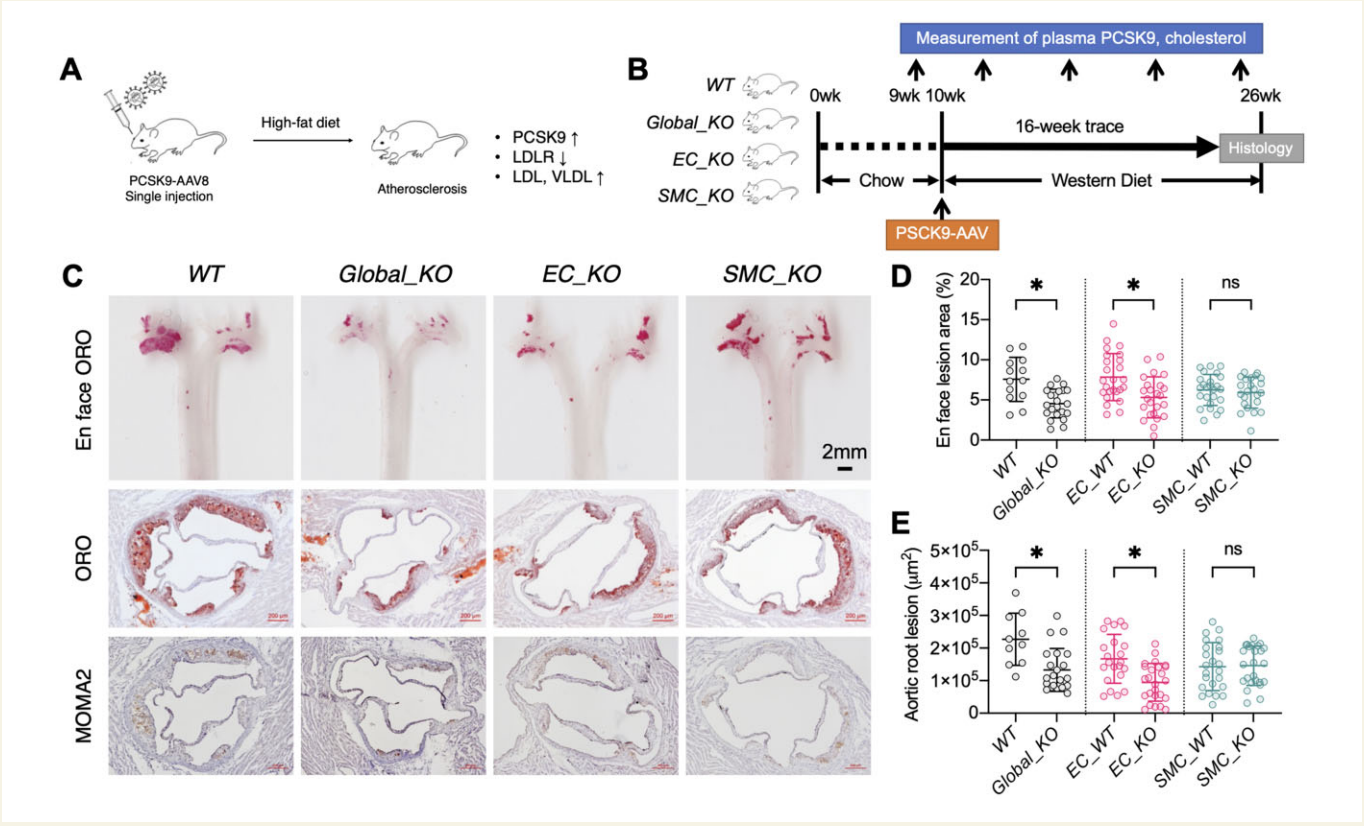

Figure 6 Deletion of ARHGEF26 in EC, but not VSMC, reduces atherosclerosis in mice. (*A*) Schematic of the murine atherosclerosis model created by a single injection of GOF PCSK9-AAV8 followed by high-fat diet. (*B*) Study design to characterize atherosclerosis susceptibility with global or tissue-specific *Arhgef26* deletion in mice. (*C*) Representative images of *en face* aortic plaque (scale = 2 mm) and aortic root sections stained with ORO (scale = 200 μm) or the monocyte/macrophage marker MOMA2 (scale = 200 μm) from mice receiving AAV-induced atherosclerosis. Note significant reduction of plaque area relative to *WT* in *global_KO* and *EC_KO* aortas, but not in *SMC_KO* aorta. Representative staining of multiple animals (exact n below and in *Figure 7C*). (*D* and *E*) Quantification of the *en face* aortic lesion area (*D*; $n = 13$, 22, 25, 24, 25, and 23, respectively) and cross-sectional aortic root lesion area (*E*; $n = 10$, 22, 22, 25, 24, and 25, respectively). All mice are male. *$P < 0.05$ by two-tailed, unpaired Student's *t*-test [$t = 3.929$, 3.206, and 0.5842; DF = 33, 47, and 46 for (*D*); $t = 3.516$, 3.726, and 0.1610; DF = 30, 45, and 47 for (*E*); ns, non-significant]. Error bars, mean ± SD.

the ARHGEF26-29Leu being a more stable protein identified by our previous work,[11] our present data showed for the first time that the differential protein interactors of the 29Leu mutant, such as MAPKs, are associated with enhanced VEGF signalling, thus further revealed the molecular mechanism underlying its mutant effect on ARHGEF26 protein. Together, our data suggests at least two distinct mechanisms account for the GOF effects of 29Leu, including enhanced protein stability and increased angiogenic activity. We considered that SNPs found in GWAS can be associated with non-coding RNAs or potential binding sites for these noncoding RNAs, However, there has been very limited data indicating an association between the sentinel SNPs of ARHGEF26 with non-coding RNAs.

A stronger interaction between ARHGEF26-29Leu and MAPK, MTA, or RBBP isoforms allows several interpretations. First, the fact that these unique protein-protein interactions and several vascular disease phenotypes have converged on the same variant is unusual, suggesting ARHGEF26 protein is disrupted in a particular way that leads to dysfunction of the vasculature. A role for the 29Leu mutant in VEGF signalling is supported by our data. However, there could be additional pathways affected by MAPK, MTA, or RBBP isoforms.

Secondly, the differential protein-protein interactions highlight the importance of a previously understudied N-terminal region of ARHGEF26. Although we did not observe a predicted NLS near the N-terminus, a proline-rich domain near 29Val has been found to recruit adaptor proteins to form heteromultimeric complexes[13] and to direct the GEF specificity to RhoG[14] by interacting with the DH domain. Truncation of the N-terminus of ARHGEF26 (including 29Val residue) markedly reduced dorsal ruffle formation in fibroblasts and abolished the RhoG-specificity of ARHGEF26.[14] Of note, our previous data has shown that 29Leu mutation has no direct effect on the GEF catalytic activity of RhoG. It is plausible that the 29Leu variant could affect GEF-independent protein interactors of RhoG or intra-molecular interactions of ARHGEF26 via altering the structure of the proline-rich domain.

Previous studies have shown a positive role of ARHGEF26 in growth factor receptor signalling. Depending on the tissue type, ARGHEF26 may enhance receptor stability,[32] alter tyrosine-phosphorylation by Src,[33] promote Fn14-receptor mediated cancer survival, or promote downstream MAPK or Akt signalling.[34,35] Among angiogenic growth factor receptors, VEGFR2 is the predominant VEGF receptor on the cell

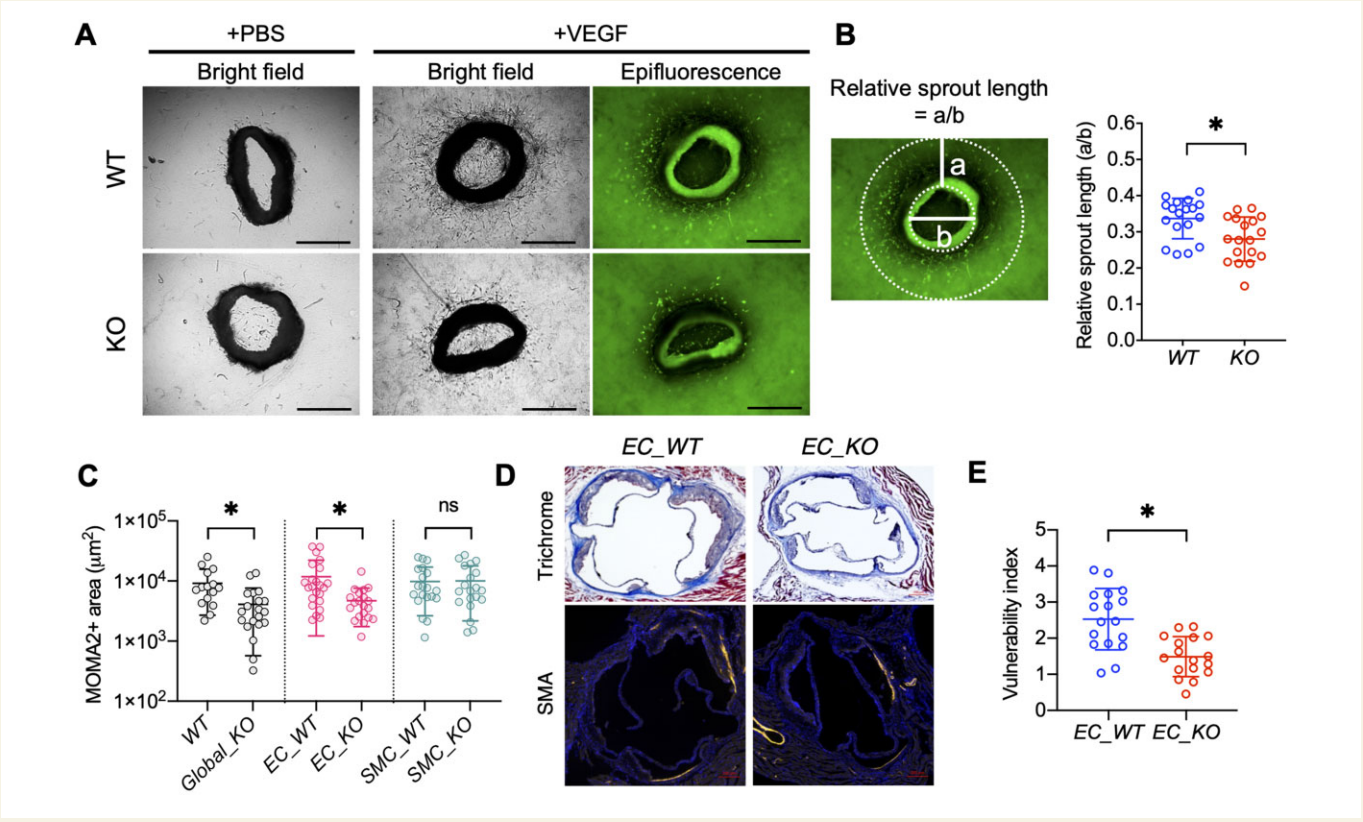

Figure 7 ARHGEF26 regulates *ex vivo* angiogenesis and plaque stability in mice. (*A*) *Ex vivo* mouse aortic ring assay. Aortic rings from *WT* and *Arhgef26−/− (KO)* mice were embedded in collagen and stimulated with PBS (control) or VEGF. The microvessel outgrowth was labelled with CellTracker Green and imaged under bright field and fluorescence on Day 4. Scale = 2 mm. (*B*) Quantification of relative sprout length, calculated as vessel length (a) divided by ring diameter (b) $n = 18$ rings per treatment (6 rings/mouse × 3 mice/genotype). *$P < 0.05$ by two-tailed, unpaired Student's t-test ($t = 2.912$, DF = 34). (*C*) quantification of the content of monocyte/macrophage by MOMA2+ area on aortic root sections of mice receiving AAV-induced atherosclerosis ($n = 15$, 20, 23, 20, 20, and 20, respectively). *$P < 0.05$ by two-tailed, unpaired Student's *t*-test ($t = 2.974$, 2.906, and 0.07233, DF = 33, 41, and 38); ns, non-significant. (*D*) Collagen content (blue) stained with Masson's Trichrome and smooth muscle cell (SMC) content (yellow) stained with α-SMA on aortic root sections of *EC_WT* and *EC_KO* mice receiving AAV-induced atherosclerosis. Scale = 200 μm. Representative of 17 mice each. (*E*) Quantification of ORO (lipid), MOMA2, collagen, and SMA staining allows comparison of plaque stability by vulnerability index between *EC_WT* and *EC_KO* mice. Vulnerability index = (monocyte/macrophage content % + lipid content %)/(collagen content % + SMC content %) ($n = 17$). *$P < 0.05$ by two-tailed, unpaired Student's *t*-test ($t = 4.204$, DF = 32). All mice are male. Error bars, mean ± SD.

surface of blood vascular EC and transduces all known effects of VEGF, whereas VEGFR1 is primarily localized in the nucleus of EC and mainly regulates cell survival.[36,37] In primary human EC, altered capillary tube formation was induced only when VEGFR2 expression was knocked down, but not VEGFR1, suggesting an absolutely essential role of VEGFR2 signalling in vascular differentiation and angiogenesis.[36] Our results suggest that in vascular EC, ARHGEF26 promotes VEGF signalling by facilitating macropinocytosis of VEGFR2, a process dependent on the expression level of RhoG. Macropinocytosis of VEGFR2 is required for VEGF-induced angiogenesis. A prior study found this process is mediated by a small GTPase CDC42 and takes place at ruffled areas of the EC membrane.[21] Additional reports show that RhoG signals upstream of CDC42 in EC,[38] forming a RhoG→CDC42 signalling cascade to further activate downstream MAPK signalling and tube formation.[39] Our results are in line with prior studies showing the RhoG-dependency in blood vessel morphogenesis[38] and that dorsal membrane ruffling, which serves as the common structural basis for both macropinocytosis and leukocyte-docking cups, is dependent on ARHGEF26.[14,15]

Elucidating the exact tissue type that permits a causal role of ARHGEF26 in atherosclerosis holds translation value. For instance, the hepatic dependency in regulating plasma lipids has enabled targeted disruption of *PCSK9*[40] and *APOC3*[41] in human liver for treatment of CAD. Importantly, highly specific and durable gene disruption targeting the endothelium has been achieved in nonhuman primates by nanoparticles without long-term adverse effects.[42] Prior studies showed that ARHGEF26 was not expressed in haematopoietic cells including monocytes, neutrophils, or platelets,[15] indicating the vasculature as the primary effect tissue for ARHGEF26 in promoting atherosclerosis. Our tissue-specific gene targeting showed that, although both EC and VSMC are known cell types contributing to a vascular lesion, it was the endothelial ARHGEF26 that determined the ultimate atherosclerotic burden *in vivo*, and that ARHGEF26 in VSMC played a minimal role. Our work highlighted a novel EC-dependent pathway that may allow targeted intervention to the vascular endothelium with existing anti-sense-nucleotide or gene-editing tools amenable to simple intravenous delivery technique.[43] We therefore anticipate our tissue-specific study could

make new preventive and therapeutic strategies for CAD more selective and efficient.

Our work has several limitations. First, we have not yet tested the effect of ARHGEF26 in models that directly observe angiogenesis *in vivo*, such as hindlimb ischaemia or retinal angiogenesis models, although we anticipate a positive effect given our *ex vivo* data; in future work, it will also be important to examine the specific role and mechanistic basis of the 29Leu mutant *in vivo* using knock-in animals of this mutation; however, such a resource is not currently available. Secondly, most atherogenic animal models, especially in small animals, exhibit profound differences in plaque characteristics as compared with humans and thus suffer from severe limitations regarding their translational value. Although the role of intraplaque angiogenesis in plaque progression is being recognized, this is mainly observed in human plaques where true ischaemia occurs, and not directly in murine lesion that lacks similar degree of ischaemia as humans. Therefore, large animal models, or more dedicated murine models may provide further translational relevance as reviewed by Perrotta *et al.*[7] Thirdly, our results do not exclude a role of ARHGEF26 in VSMC related to other vascular phenotypes, such as carotid neointima formation after balloon injury.[30] Further work is required to delineate the relative contribution of ARHGEF26 in VSMC to vascular phenotypes. Fourth, we have yet to confirm a role of ARHGEF26 on circulating risk factors of CAD. A recent report suggests that an intronic variant rs449361 within *ARHGEF26* that is in LD with rs12493885 (R^2 = 1.0 in ad mixed American; R^2 = 0.8948 in Europeans) is associated with serum uric acid level in Mexican Americans,[44] although such an association has not been found in UK Biobank. Finally, the *in vivo* role of ARHGEF26 in plaque composition must be interpreted in the context of its known effect in regulating transendothelial migration of leukocytes, which still holds true and should be considered as complementary to the angiogenic effect of ARHGEF26; both effect could partially contribute to an association between ARHGEF26 and CAD.

In summary, our work identified the role of a genetic risk factor for CAD, *ARHGEF26*, in endothelial angiogenesis, and suggested endothelial-specific inhibition of ARHGEF26 protected against atherosclerosis. Our work sheds light on a new role of ARHGEF26 specific to endothelium, generates potential therapeutic hypotheses, and may facilitate the development of new therapeutics for cardiovascular diseases.

Supplementary material

Supplementary material is available at *Cardiovascular Research* online.

Authors' contributions

Concept and design: Q.M.Z., A.L., V.K.K., S.K., and P.T.E. Acquisition, analysis, or interpretation of data: Q.M.Z., B.T.M., T.M., M.C., A.L., A.A., E.M., K.L., V.K.K., S.K., and P.T.E. Writing or critical revision of the article for important intellectual content: Q.M.Z., B.T.M., T.M., A.A., S.K., P.T.E. Administrative, technical, or material support: B.T.M., T.M., A.L., V.K.K., S.K., and P.T.E.

Acknowledgements

We thank Eric Spooner and Edward Dudek for their generous support to the proteomic work.

Conflict of interest: P.E. has received sponsored research support from Bayer AG and IBM Health. He has also served on advisory boards or consulted for Bayer AG, Quest Diagnostics, MyoKardia and Novartis. T.M. and S.K. are employees of Verve Therapeutics. S.K. holds equity in Verve Therapeutics, Maze Therapeutics, Catabasis, and San Therapeutics. He is a member of the scientific advisory boards for Regeneron Genetics Center and Corvidia Therapeutics; he has served as a consultant for Acceleron, Eli Lilly, Novartis, Merck, Novo Nordisk, Novo Ventures, Ionis, Alnylam, Aegerion, Haug Partners, Noble Insights, Leerink Partners, Bayer Healthcare, Illumina, Colour Genomics, MedGenome, Quest, and Medscape; he reports patents related to a method of identifying and treating a person having a predisposition to or afflicted with cardiometabolic disease (20180010185) and a genetics risk predictor (20190017119).

Funding

This work was supported by the Foundation Leducq (14CVD01 to P.T.E.), the National Institutes of Health (1RO1HL092577, and K24HL105780 to P.T.E.), the American Heart Association (18SFRN34110082 to P.T.E. and 19POST34380985 to Q.M.Z.), Bayer AG and Broad Institute (Broadnext10 Round 2 Award to K.L., Broadnext10 Round 3 Award to Q.M.Z.).

Data availability

The data underlying this article are available in the article and in its Supplementary Material.

References

1. Mathers CD, Loncar D. Projections of global mortality and burden of disease from 2002 to 2030. *PLoS Med* 2006;**3**:e442.
2. Benjamin EJ, Muntner P, Alonso A, Bittencourt MS, Callaway CW, Carson AP, Chamberlain AM, Chang AR, Cheng S, Das SR, Delling FN, Djousse L, Elkind MSV, Ferguson JF, Fornage M, Jordan LC, Khan SS, Kissela BM, Knutson KL, Kwan TW, Lackland DT, Lewis TT, Lichtman JH, Longenecker CT, Loop MS, Lutsey PL, Martin SS, Matsushita K, Moran AE, Mussolino ME, O'Flaherty M, Pandey A, Perak AM, Rosamond WD, Roth GA, Sampson UKA, Satou GM, Schroeder EB, Shah SH, Spartano NL, Stokes A, Tirschwell DL, Tsao CW, Turakhia MP, VanWagner LB, Wilkins JT, Wong SS, Virani SS; American Heart Association Council on Epidemiology and Prevention Statistics Committee and Stroke Statistics Subcommittee. Heart Disease and Stroke Statistics-2019 Update: a Report From the American Heart Association. *Circulation* 2019;**139**:e56–e528.
3. Erdmann J, Kessler T, Munoz Venegas L, Schunkert H. A decade of genome-wide association studies for coronary artery disease: the challenges ahead. *Cardiovasc Res* 2018;**114**:1241–1257.
4. Musunuru K, Kathiresan S. Genetics of common, complex coronary artery disease. *Cell* 2019;**177**:132–145.
5. Nelson CP, Goel A, Butterworth AS, Kanoni S, Webb TR, Marouli E, Zeng L, Ntalla I, Lai FY, Hopewell JC, Giannakopoulou O, Jiang T, Hamby SE, Di Angelantonio E, Assimes TL, Bottinger EP, Chambers JC, Clarke R, Palmer CNA, Cubbon RM, Ellinor P, Ermel R, Evangelou E, Franks PW, Grace C, Gu D, Hingorani AD, Howson JMM, Ingelsson E, Kastrati A, Kessler T, Kyriakou T, Lehtimaki T, Lu X, Lu Y, Marz W, McPherson R, Metspalu A, Pujades-Rodriguez M, Ruusalepp A, Schadt EE, Schmidt AF, Sweeting MJ, Zalloua PA, AlGhalayini K, Keavney BD, Kooner JS, Loos RJF, Patel RS, Rutter MK, Tomaszewski M, Tzoulaki I, Zeggini E, Erdmann J, Dedoussis G, Bjorkegren JLM; Epic-CVD Consortium; CardioGramplusC4D; UK Biobank CardioMetabolic CHD Working Group; Schunkert H, Farrall M, Danesh J, Samani NJ, Watkins H, Deloukas P. Association analyses based on false discovery rate implicate new loci for coronary artery disease. *Nat Genet* 2017;**49**:1385–1391.
6. Herrmann J, Lerman LO, Mukhopadhyay D, Napoli C, Lerman A. Angiogenesis in atherogenesis. *Arterioscler Thromb Vasc Biol* 2006;**26**:1948–1957.
7. Perrotta P, Emini Veseli B, Van der Veken B, Roth L, Martinet W, De Meyer GRY. Pharmacological strategies to inhibit intra-plaque angiogenesis in atherosclerosis. *Vascul Pharmacol* 2019;**112**:72–78.
8. Winter PM, Neubauer AM, Caruthers SD, Harris TD, Robertson JD, Williams TA, Schmieder AH, Hu G, Allen JS, Lacy EK, Zhang H, Wickline SA, Lanza GM. Endothelial alpha(v)beta3 integrin-targeted fumagillin nanoparticles inhibit angiogenesis in atherosclerosis. *Arterioscler Thromb Vasc Biol* 2006;**26**:2103–2109.

9. Epstein SE, Stabile E, Kinnaird T, Lee CW, Clavijo L, Burnett MS. Janus phenomenon: the interrelated tradeoffs inherent in therapies designed to enhance collateral formation and those designed to inhibit atherogenesis. *Circulation* 2004;**109**:2826–2831.
10. Sluimer JC, Daemen MJ. Novel concepts in atherogenesis: angiogenesis and hypoxia in atherosclerosis. *J Pathol* 2009;**218**:7–29.
11. Klarin D, Zhu QM, Emdin CA, Chaffin M, Horner S, McMillan BJ, Leed A, Weale ME, Spencer CCA, Aguet F, Segre AV, Ardlie KG, Khera AV, Kaushik VK, Natarajan P; CARDIoGRAMplusC4D ConsortiumKathiresan S. Genetic analysis in UK Biobank links insulin resistance and transendothelial migration pathways to coronary artery disease. *Nat Genet* 2017;**49**:1392–1397.
12. Verweij N, Eppinga RN, Hagemeijer Y, van der Harst P. Identification of 15 novel risk loci for coronary artery disease and genetic risk of recurrent events, atrial fibrillation and heart failure. *Sci Rep* 2017;**7**:2761.
13. Qi H, Fournier A, Grenier J, Fillion C, Labrie Y, Labrie C. Isolation of the novel human guanine nucleotide exchange factor Src homology 3 domain-containing guanine nucleotide exchange factor (SGEF) and of C-terminal SGEF, an N-terminally truncated form of SGEF, the expression of which is regulated by androgen in prostate cancer cells. *Endocrinology* 2003;**144**:1742–1752.
14. Ellerbroek SM, Wennerberg K, Arthur WT, Dunty JM, Bowman DR, DeMali KA, Der C, Burridge K. SGEF, a RhoG guanine nucleotide exchange factor that stimulates macropinocytosis. *Mol Biol Cell* 2004;**15**:3309–3319.
15. Samson T, van Buul JD, Kroon J, Welch C, Bakker EN, Matlung HL, van den Berg TK, Sharek L, Doerschuk C, Hahn K, Burridge K. The guanine-nucleotide exchange factor SGEF plays a crucial role in the formation of atherosclerosis. *PLoS One* 2013;**8**:e55202.
16. van Rijssel J, Kroon J, Hoogenboezem M, van Alphen FP, de Jong RJ, Kostadinova E, Geerts D, Hordijk PL, van Buul JD. The Rho-guanine nucleotide exchange factor Trio controls leukocyte transendothelial migration by promoting docking structure formation. *Mol Biol Cell* 2012;**23**:2831–2844.
17. van Buul JD, Allingham MJ, Samson T, Meller J, Boulter E, Garcia-Mata R, Burridge K. RhoG regulates endothelial apical cup assembly downstream from ICAM1 engagement and is involved in leukocyte trans-endothelial migration. *J Cell Biol* 2007;**178**:1279–1293.
18. Brinkman EK, Chen T, Amendola M, van Steensel B. Easy quantitative assessment of genome editing by sequence trace decomposition. *Nucl Acids Res* 2014;**42**:e168.
19. Nakatsu MN, Davis J, Hughes CC. Optimized fibrin gel bead assay for the study of angiogenesis. *J Vis Exp* 2007;**3**:186.
20. Rioja AY, Tiruvannamalai Annamalai R, Paris S, Putnam AJ, Stegemann JP. Endothelial sprouting and network formation in collagen- and fibrin-based modular microbeads. *Acta Biomater* 2016;**29**:33–41.
21. Basagiannis D, Zografou S, Murphy C, Fotsis T, Morbidelli L, Ziche M, Bleck C, Mercer J, Christoforidis S. VEGF induces signalling and angiogenesis by directing VEGFR2 internalisation through macropinocytosis. *J Cell Sci* 2016;**129**:4091–4104.
22. Lanahan A, Zhang X, Fantin A, Zhuang Z, Rivera-Molina F, Speichinger K, Prahst C, Zhang J, Wang Y, Davis G, Toomre D, Ruhrberg C, Simons M. The neuropilin 1 cytoplasmic domain is required for VEGF-A-dependent arteriogenesis. *Dev Cell* 2013;**25**:156–168.
23. Petazzi P, Sandoval J, Szczesna K, Jorge OC, Roa L, Sayols S, Gomez A, Huertas D, Esteller M. Dysregulation of the long non-coding RNA transcriptome in a Rett syndrome mouse model. *RNA Biol* 2013;**10**:1197–1203.
24. McCauley MD, Wang T, Mike E, Herrera J, Beavers DL, Huang TW, Ward CS, Skinner S, Percy AK, Glaze DG, Wehrens XH, Neul JL. Pathogenesis of lethal cardiac arrhythmias in Mecp2 mutant mice: implication for therapy in Rett syndrome. *Sci Transl Med* 2011;**3**:113ra125.
25. Mashiko D, Fujihara Y, Satouh Y, Miyata H, Isotani A, Ikawa M. Generation of mutant mice by pronuclear injection of circular plasmid expressing Cas9 and single guided RNA. *Sci Rep* 2013;**3**:3355.
26. Richardson CD, Ray GJ, DeWitt MA, Curie GL, Corn JE. Enhancing homology-directed genome editing by catalytically active and inactive CRISPR-Cas9 using asymmetric donor DNA. *Nat Biotechnol* 2016;**34**:339–344.
27. Aida T, Chiyo K, Usami T, Ishikubo H, Imahashi R, Wada Y, Tanaka KF, Sakuma T, Yamamoto T, Tanaka K. Cloning-free CRISPR/Cas system facilitates functional cassette knock-in in mice. *Genome Biol* 2015;**16**:87.
28. Bjorklund MM, Hollensen AK, Hagensen MK, Dagnaes-Hansen F, Christoffersen C, Mikkelsen JG, Bentzon JF. Induction of atherosclerosis in mice and hamsters without germline genetic engineering. *Circ Res* 2014;**114**:1684–1689.
29. Bowling MR, Xing D, Kapadia A, Chen YF, Szalai AJ, Oparil S, Hage FG. Estrogen effects on vascular inflammation are age dependent: role of estrogen receptors. *Arterioscler Thromb Vasc Biol* 2014;**34**:1477–1485.
30. Zahedi F, Nazari-Jahantigh M, Zhou Z, Subramanian P, Wei Y, Grommes J, Offermanns S, Steffens S, Weber C, Schober A. Dicer generates a regulatory microRNA network in smooth muscle cells that limits neointima formation during vascular repair. *Cell Mol Life Sci* 2017;**74**:359–372.
31. Miano JM, Zhu QM, Lowenstein CJ. A CRISPR path to engineering new genetic mouse models for cardiovascular research. *Arterioscler Thromb Vasc Biol* 2016;**36**:1058–1075.
32. Wang H, Li S, Li H, Li C, Guan K, Luo G, Yu L, Wu R, Zhang X, Wang J, Zhou J. SGEF enhances EGFR stability through delayed EGFR trafficking from early to late endosomes. *Carcinogenesis* 2013;**34**:1976–1983.
33. Okuyama Y, Umeda K, Negishi M, Katoh H. Tyrosine phosphorylation of SGEF regulates RhoG activity and cell migration. *PLoS One* 2016;**11**:e0159617.
34. Wang H, Li S, Li H, Wang P, Huang F, Zhao Y, Yu L, Luo G, Zhang X, Wang J, Zhou J. Grb2 interacts with SGEF and antagonizes the ability of SGEF to enhance EGF-induced ERK1/2 activation. *Mol Cell Biochem* 2014;**389**:239–247.
35. Wang H, Wu R, Yu L, Wu F, Li S, Zhao Y, Li H, Luo G, Wang J, Zhou J. SGEF is overexpressed in prostate cancer and contributes to prostate cancer progression. *Oncol Rep* 2012;**28**:1468–1474.
36. Zhang Z, Neiva KG, Lingen MW, Ellis LM, Nor JE. VEGF-dependent tumor angiogenesis requires inverse and reciprocal regulation of VEGFR1 and VEGFR2. *Cell Death Differ* 2010;**17**:499–512.
37. Simons M, Gordon E, Claesson-Welsh L. Mechanisms and regulation of endothelial VEGF receptor signalling. *Nat Rev Mol Cell Biol* 2016;**17**:611–625.
38. Abraham S, Scarcia M, Bagshaw RD, McMahon K, Grant G, Harvey T, Yeo M, Esteves FO, Thygesen HH, Jones PF, Speirs V, Hanby AM, Selby PJ, Lorger M, Dear TN, Pawson T, Marshall CJ, Mavria G. A Rac/Cdc42 exchange factor complex promotes formation of lateral filopodia and blood vessel lumen morphogenesis. *Nat Commun* 2015;**6**:7286.
39. El Atat O, Fakih A, El-Sibai M. RHOG activates RAC1 through CDC42 leading to tube formation in vascular endothelial cells. *Cells* 2019;**8**:171.
40. Fitzgerald K, White S, Borodovsky A, Bettencourt BR, Strahs A, Clausen V, Wijngaard P, Horton JD, Taubel J, Brooks A, Fernando C, Kauffman RS, Kallend D, Vaishnaw A, Simon A. A highly durable RNAi therapeutic inhibitor of PCSK9. *N Engl J Med* 2017;**376**:41–51.
41. Gaudet D, Alexander VJ, Baker BF, Brisson D, Tremblay K, Singleton W, Geary RS, Hughes SG, Viney NJ, Graham MJ, Crooke RM, Witztum JL, Brunzell JD, Kastelein JJ. Antisense inhibition of apolipoprotein C-III in patients with hypertriglyceridemia. *N Engl J Med* 2015;**373**:438–447.
42. Khan OF, Kowalski PS, Doloff JC, Tsosie JK, Bakthavatchalu V, Winn CB, Haupt J, Jamiel M, Langer R, Anderson DG. Endothelial siRNA delivery in nonhuman primates using ionizable low-molecular weight polymeric nanoparticles. *Sci Adv* 2018;**4**:eaar8409.
43. Alaarg A, Perez-Medina C, Metselaar JM, Nahrendorf M, Fayad ZA, Storm G, Mulder WJM. Applying nanomedicine in maladaptive inflammation and angiogenesis. *Adv Drug Deliv Rev* 2017;**119**:143–158.
44. Chittoor G, Kent JW Jr, Almeida M, Puppala S, Farook VS, Cole SA, Haack K, Goring HH, MacCluer JW, Curran JE, Carless MA, Johnson MP, Moses EK, Almasy L, Mahaney MC, Lehman DM, Duggirala R, Comuzzie AG, Blangero J, Voruganti VS. GWAS and transcriptional analysis prioritize ITPR1 and CNTN4 for a serum uric acid 3p26 QTL in Mexican Americans. *BMC Genomics* 2016;**17**:276.

Translational perspective

Understanding the genetic architecture of coronary artery disease (CAD) is critical to developing new therapeutics. Here, we present work that revealed the causal mechanism by which DNA variants at the *ARHGEF26* locus confer risk for CAD. Angiogenesis-related vascular phenotypes are associated with the *ARHGEF26* locus, and ARHGEF26 promotes the angiogenic capacity of human endothelial cells. Together, our work demonstrates that ARHGEF26 is a novel angiogenic factor, and endothelial-specific inhibition of ARHGEF26 may be beneficial to treating CAD. The causal pathway and the actionable therapeutic hypotheses from our work will facilitate the development of new therapeutics for CAD.